Analytical Solution of 1-Dimensional Peridynamic Equation of Motion

Zhenghao Yang[1,*], Chien-Ching Ma[1], Erkan Oterkus[2], Selda Oterkus[2], Konstantin Naumenko[3]

[1]Department of Mechanical Engineering, National Taiwan University, Taipei, Taiwan

[2]PeriDynamics Research Centre, Department of Naval Architecture, Ocean and Marine Engineering, University of Strathclyde, Glasgow, United Kingdom

[3]Otto von Guericke University, Institute of Mechanics, Magdeburg, Germany

Abstract

Peridynamics has been introduced to overcome limitations of classical continuum mechanics. Peridynamic equations of motion are in the form of integro-differential equations and analytical solutions of these equations are limited in the literature. In this study, a new analytical solution methodology for 1-Dimensional peridynamic equation of motion is presented by utilising inverse Fourier Transform. Analytical solutions for both static and dynamic conditions are obtained. Moreover, different boundary conditions including fixed-fixed and fixed-free are considered. Several numerical cases are demonstrated to show the capability of the presented methodology and peridynamic results are compared against results obtained from classical continuum mechanics. A very good agreement between these two different approaches is observed which shows the capability of the current approach.

Keywords: peridynamics; non-local; analytical; one-dimensional

1. Introduction

Peridynamics (PD) [1, 2] is a new continuum mechanics formulation which was developed to overcome the limitations of classical continuum mechanics (CCM). PD equations have the form of integro-differential equations as opposed to CCM which is based on partial differential equations. This allows natural treatment of discontinuities in the displacement field due to existence or occurrence of cracks. In addition, interactions between material points in PD are not limited to nearest neighbours as in CCM and material points inside an influence domain, named as horizon, can interact with each other. The size of horizon can be considered as length scale parameter which extends the application scope of PD.

There has been a significant progress in PD especially during recent years. PD has been used for prediction of damage in different material systems such as metals [3], composites [4,5], concrete [6,7], functionally graded materials [8,9], graphene [10,11], ice [12,13], etc. In addition to elastic material behaviour, it is possible to consider plasticity [14], viscoelasticity [15] and viscoplasticity [16] in PD framework. Moreover, PD formulations are also available for simplified structures such as beams [17,18], plates [19-21] and shells [22]. PD has also been utilised for the investigation of fatigue damage [23,24], buckling [25], topology optimisation [26], dynamic crack arrest [27], macro crack and micro crack interactions [28]. PD has also been used for the analysis of moisture diffusion [29] and corrosion damage [30,31]. A comprehensive review on peridynamics can be found in [32].

Analytical solution of PD equations is limited in the literature. Mikata [33] developed analytical solutions of peristatic and peridynamic problems for a 1-Dimensional rod. In another study, Mikata [34] derived analytical solution for peridynamic equation for acoustics. Silling et. al. [35] investigated the deformation of an infinite bar subjected to a self-equilibrated load distribution by utilising peridynamic formulation and obtaining solution via Fourier transform methods. Weckner and Abeyaratne [36] examined the one-dimensional dynamic response of an infinite bar by considering the effects of long-range forces and utilising peridynamics. In a separate study, Weckner et. al. [37] used Laplace and Fourier transforms and obtained three-dimensional

*Corresponding author: yangzh2006@hotmail.com

peridynamic equations by utilising Green's functions. Aksoylu and Gazonas [38] provided a comprehensive treatment on how to enforce inhomogeneous local boundary conditions in 1-Dimensional nonlocal problems and presented exact solutions.

In this study, a new way of obtaining analytical solution to 1-Dimensional peridynamic equation of motion is presented by utilising inverse Fourier transform. Analytical solutions are obtained both for static and dynamic conditions. Two different boundary conditions are considered as fixed-fixed and fixed-free. Peridynamic solutions are validated by comparing against classical continuum mechanics solutions.

2. Analytical Solution of 1-Dimensional Peridynamic Equation of Motion

PD governing equation for a 1-Dimensional rod under static conditions can be expressed as

$$c\int_{H_x}\frac{u(x+\xi)-u(x)}{|\xi|}d\xi+f(x)=0\quad(0<x<L) \tag{1}$$

in which $c=\frac{2E}{\delta^2}$ represents the PD material constant, E is elastic modulus, H_x and δ represent the horizon and horizon size, ξ is the local coordinate, and $f(x)$ is the body load.

Assuming the solution to Eq. (1), $u(x)\in C^2([0,L])$ exists in the Hilbert space spanned by basis of trigonometric functions, i.e.

$$u(x)\in Span\left\{\begin{matrix}\frac{1}{\sqrt{2}}, & \cos(sx), & \cos(2sx), & \cos(3sx), & ...\\ & \sin(sx), & \sin(2sx), & \sin(3sx), & ...\end{matrix}\right\} \tag{2}$$

where $s\in\mathbb{R}$ is the indeterminate coefficient and decomposing the displacement function, $u(x)$, into components by using the basis functions given in Eq. (2) yields:

$$u(x)=\frac{a_0}{2}+\sum_{n=1}^{\infty}a_n\cos(nsx)+b_n\sin(nsx) \tag{3}$$

where a_n and b_n $(n=0,1,2,...)$ are the projection of $u(x)$ onto the basis $\cos(nsx)$ and $\sin(nsx)$, respectively, such that

$$a_n=\langle u(x),\cos(nsx)\rangle \tag{4a}$$

and

$$b_n=\langle u(x),\sin(nsx)\rangle \tag{4b}$$

Substituting Eq. (3) into Eq. (1) yields

$$c\sum_{n=1}^{\infty}\int_{H_x}\frac{a_n\cos\left[ns(x+\xi)\right]+b_n\sin\left[ns(x+\xi)\right]-a_n\cos(nsx)-b_n\sin(nsx)}{|\xi|}d\xi+f(x)=0 \tag{5}$$

which can be using the trigonometric identities as

$$\begin{aligned}&c\sum_{n=1}^{\infty}a_n\int_{H_x}\frac{\cos(nsx)\left[\cos(ns\xi)-1\right]-\sin(nsx)\sin(ns\xi)}{|\xi|}d\xi\\&+c\sum_{n=1}^{\infty}b_n\int_{H_x}\frac{\sin(nsx)\left[\cos(ns\xi)-1\right]+\cos(nsx)\sin(ns\xi)}{|\xi|}d\xi+f(x)=0\end{aligned} \tag{6}$$

Note that if there is no bond damage associated with the material point x, in other words the horizon $H_x = (-\delta, \delta)$ is intact, Eq. (6) can be further reduced to

$$c\sum_{n=1}^{\infty} a_n \cos(nsx)\int_{-\delta}^{\delta} \frac{\cos(ns\xi)-1}{|\xi|} d\xi + c\sum_{n=1}^{\infty} b_n \sin(nsx)\int_{-\delta}^{\delta} \frac{\cos(ns\xi)-1}{|\xi|} d\xi + f(x) = 0 \tag{7}$$

where the coefficients a_n and b_n can be determined as

$$a_n = \frac{s}{c\pi} \frac{\int_0^{\frac{\pi}{s}} f(x)\cos(nsx)dx}{\int_{-\delta}^{\delta} \frac{1-\cos(ns\xi)}{|\xi|} d\xi} \tag{8a}$$

and

$$b_n = \frac{s}{c\pi} \frac{\int_0^{\frac{\pi}{s}} f(x)\sin(nsx)dx}{\int_{-\delta}^{\delta} \frac{1-\cos(ns\xi)}{|\xi|} d\xi} \tag{8b}$$

Coupling Eqs. (8a) and (8b) with Eq. (3) yields

$$u(x) = \frac{a_0}{2} + \frac{s}{c\pi}\sum_{n=1}^{\infty}\left[\frac{\int_0^{\frac{\pi}{s}} f(x)\cos(nsx)dx}{\int_{-\delta}^{\delta} \frac{1-\cos(ns\xi)}{|\xi|} d\xi}\cos(nsx) + \frac{\int_0^{\frac{\pi}{s}} f(x)\sin(nsx)dx}{\int_{-\delta}^{\delta} \frac{1-\cos(ns\xi)}{|\xi|} d\xi}\sin(nsx) \right] \tag{9}$$

Eq. (9) is called the general solution to PD 1D static formulation, where the parameter a_0 and s depend upon rigid body motion and boundary conditions, respectively.

3. Peridynamic Boundary Conditions

From PD point of view, except damage situation, each material point must be completely embedded in its PD influence domain. Moreover, for those material points adjacent to the boundary, whose domain is incomplete, it is necessary to introduce fictitious region outside the boundary such that the validation of PD Equation of Motion (EoM) is ensured. The width of fictitious region can be chosen as equal to the horizon size δ, as shown in Fig. 1. Two types of BCs and their implementation in PD framework are explained below.

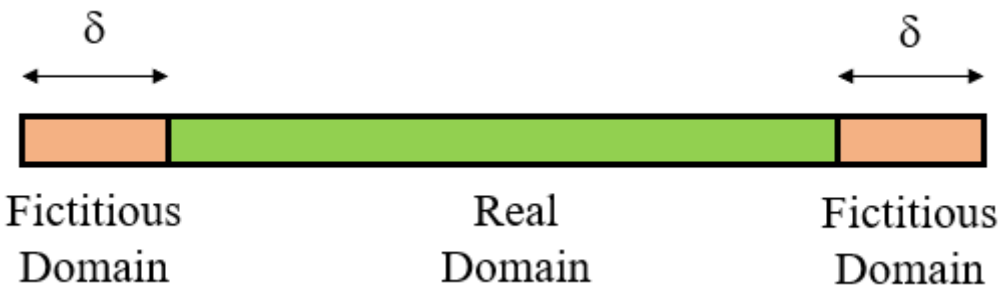

Figure 1. Real and fictitious domains

3.1 Fixed Boundary Conditions

Recall the EoM in classical elasticity:

$$\rho\ddot{u}(x,t) = E\frac{\partial^2 u(x,t)}{\partial x^2} + b(x,t) \quad 0 < x < L \tag{10}$$

Suppose the body is constrained at $x = 0$ such that $u(0,t) \equiv 0$, the representation of Eq. (10) at this point is:

$$E\frac{\partial^2 u(x,t)}{\partial x^2}\bigg|_{x=0} = 0 \tag{11}$$

One can obtain by performing central difference for Eq. (11) that

$$E\frac{u(-\Delta x,t) - 2u(0,t) + u(\Delta x,t)}{(\Delta x)^2} = 0 \tag{12}$$

where Δx is incremental distance. Simplifying Eq. (12) and swapping the difference notation Δx by ξ leads to

$$u(-\xi,t) = -u(\xi,t) \quad 0 \le \xi \le \delta \tag{13}$$

Here, the material point $x = -\xi$ lies in the fictitious region and Eq. (13) holds for $\xi = 0$ which ensures the fixed BC, $u(0) = 0$, is satisfied for PD EoM.

3.2 Neumann Boundary Conditions

Suppose the body is subjected to a concentrated load of $p(t)$ at $x = L$. In classical elasticity theory, the boundary condition can be represented as

$$\sigma(L,t) = E\frac{\partial u(x,t)}{\partial x}\bigg|_{x=L} = p(t) \tag{14}$$

Again, performing central difference with respect to u gives

$$E\frac{u(L+\Delta x,t) - u(L-\Delta x,t)}{2\Delta x} = p(t) \tag{15}$$

After performing some algebra and rearranging the central difference notation according to PD convention, one can obtain that

$$u(L+\xi,t) = 2\frac{p(t)}{E}\xi + u(L-\xi,t) \quad 0 \le \xi \le \delta \tag{16}$$

Note that Eq. (16) holds for $\xi = 0$ to ensure the continuity of displacement field at the boundary, and $p(t)$ can be eliminated from Eq. (16) and absorbed in Eq. (10) if it is considered as the body force operated by Dirac delta. According to this point of view, Eq. (16) reduces to

$$u(L+\xi,t) = u(L-\xi,t) \quad 0 \le \xi \le \delta \tag{17}$$

and Eq. (17) is called the free boundary condition relationship in PD framework.

4. Static Peridynamic Solution

4.1 Dirichlet Boundary Condition (Fixed – Fixed)

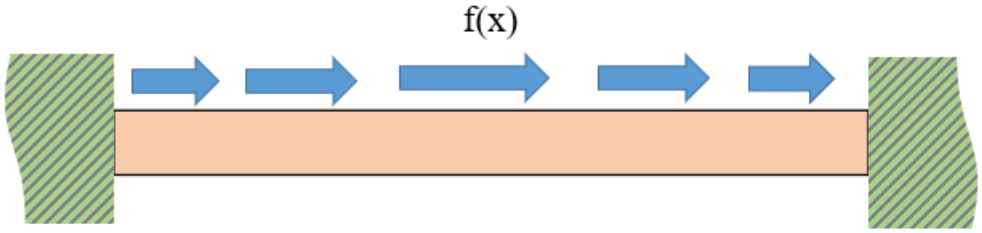

Figure 2. A rod under fixed-fixed boundary conditions and subjected to an arbitrary force field.

Suppose a rod with a length of L is subjected to an arbitrary body force field and constrained at two ends, as shown in Fig. 2. As explained above, two fictitious regions can be introduced outside the two boundary ends. The governing equation and BCs can be expressed as

$$c\int_{-\delta}^{\delta}\frac{u(x+\xi)-u(x)}{|\xi|}d\xi+f(x)=0 \quad (0<x<L) \tag{18}$$

$$\text{BCs: } \begin{cases} u(x)=-u(-x) & \forall x\in[0,\delta] \\ u(L-x)=-u(L+x) & \forall x\in[L,L+\delta] \end{cases} \tag{19a,b}$$

Periodically extending the BC given in Eq. (19a) over the entire real line, as shown in Fig. 3,

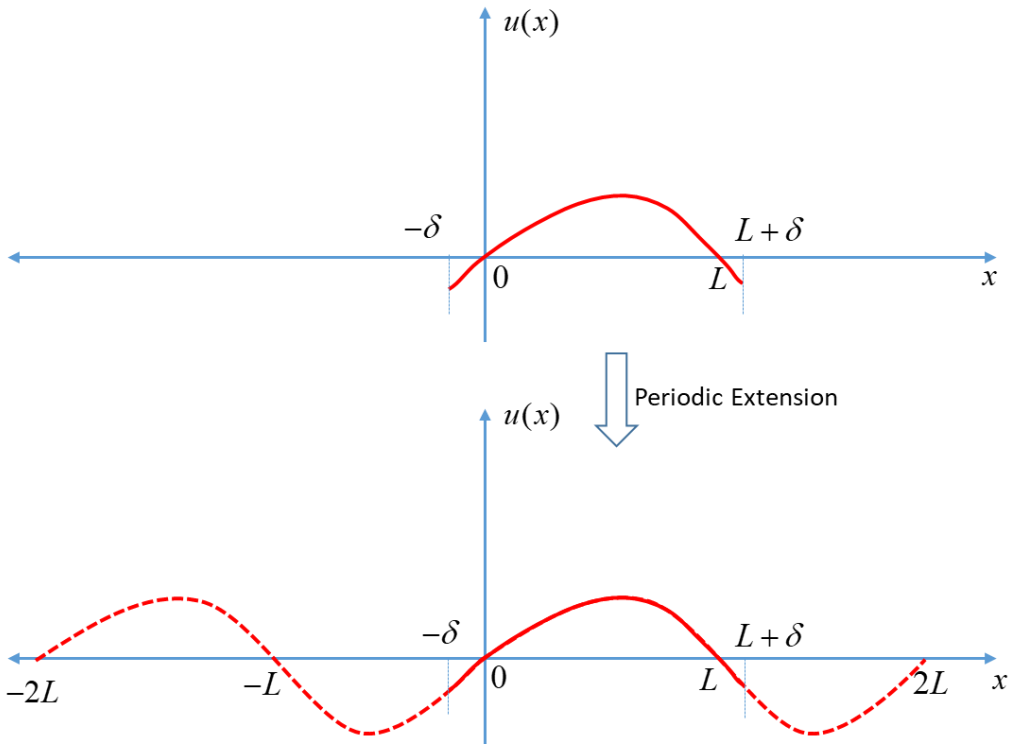

Figure 3. Periodically extended BC over the entire real line.

indicates that the displacement function, Eq. (3) is odd with respect to $x=0$ and $x=L$, which implies

$$\begin{cases} a_0=a_n=0 \quad n=1,2,3,... \\ s=\dfrac{\pi}{L} \end{cases} \Rightarrow \quad u(x)=\sum_{n=1}^{\infty}b_n\sin\left(\frac{n\pi}{L}x\right) \tag{20}$$

Coupling Eq. (20), with (8b) and (9) results in the PD analytic solution as

$$u(x)=\frac{2}{cL}\sum_{n=1}^{\infty}\frac{\int_0^L f(x)\sin\left(\frac{n\pi x}{L}\right)dx}{\int_{-\delta}^{\delta}\frac{1}{|\xi|}\left[1-\cos\left(\frac{n\pi\xi}{L}\right)\right]d\xi}\sin\left(\frac{n\pi x}{L}\right) \tag{21}$$

4.2 Fixed-Free Boundary Condition

Suppose a fixed-free rod subjected to an arbitrary body force field over the body, as shown in Fig. 4.

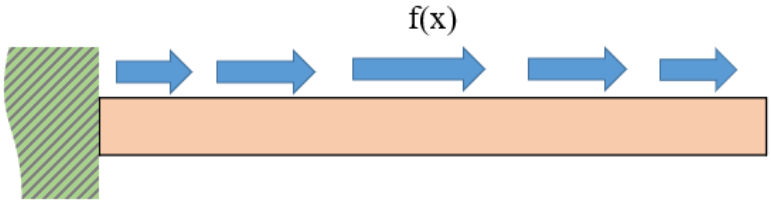

Figure 4. A rod under fixed-free boundary conditions and subjected to an arbitrary force field.

Without loss of generality, let the origin located at the fixed end. As explained above, the PD governing equation and BCs can be expressed as

$$c\int_{-\delta}^{\delta}\frac{u(x+\xi)-u(x)}{|\xi|}d\xi+f(x)=0 \quad (0<x<L) \tag{22}$$

$$\text{BCs: } \begin{cases} u(x)=-u(-x) & \forall x\in[0,\delta] \\ u(L-x)=u(L+x) & \forall x\in[0,\delta] \end{cases} \tag{23a,b}$$

By obeying the relation given in Eq. (23), we can periodically extend the displacement field over the entire real line as shown in Fig. 5

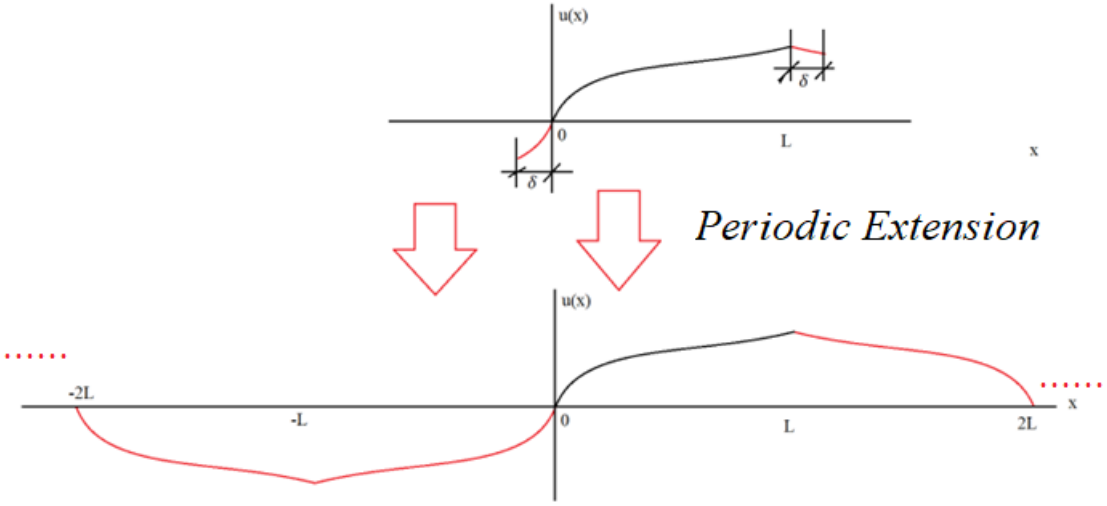

Figure 5. Periodically extended BC over the entire real line.

which reduces Eq. (3) as

$$\begin{cases} a_0 = a_n = 0 \quad n = 1,2,3,... \\ s = \dfrac{2n-1}{2n}\dfrac{\pi}{L} \end{cases} \Rightarrow \quad u(x) = \sum_{n=1}^{\infty} b_n \sin\left(\frac{2n-1}{2}\frac{\pi}{L}x\right) \tag{24}$$

Plugging Eq. (24) back into Eq. (3) and (8b) yields the PD analytical solution for fixed-free rod as:

$$u(x) = \sum_{n=1}^{\infty} \frac{2}{cL} \frac{\int_0^L f(x)\sin\left(\dfrac{(2n-1)\pi x}{2L}\right)dx}{\int_{-\delta}^{\delta} \dfrac{1}{|\xi|}\left[1-\cos\left(\dfrac{(2n-1)\pi\xi}{2L}\right)\right]d\xi} \sin\left(\frac{(2n-1)\pi x}{2L}\right) \tag{25}$$

5. Dynamic Peridynamic Solution

So far only static condition has been considered. The dynamic PD EoM can be written as:

$$\rho\ddot{u}(x,t) = c\int_{-\delta}^{\delta} \frac{u(x+\xi,t)-u(x,t)}{|\xi|}d\xi \tag{26}$$

According to the theory of structural vibrations, solution to Eq. (33) can be reasonably constructed as superposition of each vibrational mode. By performing the separation of variable method and considering linear superposition principle, solution to Eq. (26) can be assumed as

$$u(x,t) = X(x)T(t) = \sum_{n=1}^{\infty} X_n(x)T_n(t) \tag{27}$$

By plugging Eq. (27) back into (26) yields

$$\rho X(x)\ddot{T}(t) = c\int_{-\delta}^{\delta} \frac{X(x+\xi)T(t)-X(x)T(t)}{|\xi|}d\xi \tag{28}$$

and rearranging the terms yields

$$\frac{\rho}{c}\frac{\ddot{T}(t)}{T(t)} = \frac{1}{X(x)}\int_{-\delta}^{\delta} \frac{X(x+\xi)-X(x)}{|\xi|}d\xi = -\lambda \tag{29}$$

which can be separately written as:

$$\frac{\rho}{c}\frac{\ddot{T}(t)}{T(t)} = -\lambda \tag{30a}$$

and

$$\int_{-\delta}^{\delta} \frac{X(x+\xi)-X(x)}{|\xi|}d\xi = -\lambda X(x) \tag{30b}$$

in which λ can be called a ‘’pseudo eigenvalue’’ and is a constant with respect to variables x and t. Based on the linearity of the system, each vibration mode of the body should also satisfy the characteristic functions given in Eqs. (30a) and (30b) such that

$$\frac{\rho}{c}\frac{\ddot{T}_n(t)}{T_n(t)} = -\lambda_n \tag{31a}$$

and

$$\int_{-\delta}^{\delta} \frac{X_n(x+\xi)-X_n(x)}{|\xi|} d\xi = -\lambda_n X_n(x) \tag{31b}$$

where the suffix n denotes the n^{th} vibration mode. With the help of the completeness of trigonometric system, one can assume that $\forall t = t'$, $t' \geq 0$, the displacement field $u(x,t')$ lies in the function space spanning the basis of trigonometric functions such that

$$u(x,t') \in Span\left\{ \begin{matrix} \frac{1}{\sqrt{2}}, & \cos(sx), & \cos(2sx), & \cos(3sx), & ... \\ & \sin(sx), & \sin(2sx), & \sin(3sx), & ... \end{matrix} \right\} \tag{32}$$

Therefore, irrespective of rigid body motion the modal shape function can be expressed as

$$X_n(x) = a_n \cos(nsx) + b_n \sin(nsx) \tag{33}$$

Substituting Eq. (33) into (31b) results in the n^{th} ''pseudo eigenvalue'' as

$$\lambda_n = \int_{-\delta}^{\delta} \frac{1-\cos(ns\xi)}{|\xi|} d\xi \tag{34}$$

Apparently from Eq. (34) we know that λ_n is always positive. The general solution to Eq. (31b) thus can be written as

$$T_n(t) = A_n \sin\left(\sqrt{\lambda_n \frac{c}{\rho}} t\right) + B_n \cos\left(\sqrt{\lambda_n \frac{c}{\rho}} t\right) \tag{35}$$

Coupling Eq. (33) and (35) with (27) induces the PD general solution as

$$u(x,t) = \sum_{n=1}^{\infty} \left[a_n \cos(nsx) + b_n \sin(nsx) \right] \left[A_n \cos\left(\sqrt{\lambda_n \frac{c}{\rho}} t\right) + B_n \sin\left(\sqrt{\lambda_n \frac{c}{\rho}} t\right) \right] \tag{36}$$

where s, a_n, b_n, A_n and B_n are undetermined parameters depending upon boundary conditions and initial conditions.

5.1 Fixed-Fixed Boundary Condition

PD EoM, Initial Conditions (ICs) & Boundary Conditions (BCs) can be written for fixed-fixed condition as:

$$\rho \ddot{u}(x,t) = c \int_{-\delta}^{\delta} \frac{u(x+\xi,t)-u(x,t)}{|\xi|} d\xi \quad 0 \leq x \leq L \tag{37}$$

$$\text{BCs: } \begin{cases} u(-x,t) = -u(x,t) & 0 \leq x \leq \delta \\ u(L+x,t) = -u(L-x,t) & 0 \leq x \leq \delta \end{cases} \tag{38a,b}$$

$$\text{ICs: } \begin{cases} u(x,0) = u_0(x) \\ \dot{u}(x,t)\big|_{t=0} = v_0(x) \end{cases} \tag{39a,b}$$

Periodically extending Eq. (38a, b) by imitating Section 4.1 and substituting into (36), one can obtain that

$$a_n = 0 \tag{40a}$$

and

$$s = \frac{\pi}{L} \tag{40b}$$

Thus Eq. (36) reduces to

$$u(x,t) = \sum_{n=1}^{\infty} \left[A_n \cos\left(\sqrt{\lambda_n \frac{c}{\rho}} t \right) + B_n \sin\left(\sqrt{\lambda_n \frac{c}{\rho}} t \right) \right] \sin\left(\frac{n\pi x}{L} \right) \tag{41a}$$

and its derivative with respect to t is

$$\dot{u}(x,t) = \sum_{n=1}^{\infty} \sqrt{\lambda_n \frac{c}{\rho}} \left[B_n \cos\left(\sqrt{\lambda_n \frac{c}{\rho}} t \right) - A_n \sin\left(\sqrt{\lambda_n \frac{c}{\rho}} t \right) \right] \sin\left(\frac{n\pi x}{L} \right) \tag{42b}$$

Applying ICs Eq. (39a, b) to (42a, b) gives:

$$u_0(x) = \sum_{n=1}^{\infty} A_n \sin\left(\frac{n\pi x}{L} \right) \tag{43a}$$

and

$$v_0(x) = \sum_{n=1}^{\infty} \sqrt{\lambda_n \frac{c}{\rho}} B_n \sin\left(\frac{n\pi x}{L} \right) \tag{43b}$$

The coefficients A_n and B_n in Eq. (43a, b) can be determined by performing inverse Fourier transform as

$$A_n = \frac{2}{L} \int_0^L u_0(x) \sin\left(\frac{n\pi x}{L} \right) dx \tag{44a}$$

and

$$B_n = \frac{1}{\sqrt{\lambda_n \frac{c}{\rho}}} \frac{2}{L} \int_0^L v_0(x) \sin\left(\frac{n\pi x}{L} \right) dx \tag{44b}$$

Overall, the PD explicit solution is:

$$u(x,t) = \sum_{n=1}^{\infty} \left[A_n \cos\left(\sqrt{\lambda_n \frac{c}{\rho}} t \right) + B_n \sin\left(\sqrt{\lambda_n \frac{c}{\rho}} t \right) \right] \sin\left(\frac{n\pi x}{L} \right)$$

with

$$A_n = \frac{2}{L} \int_0^L u_0(x) \sin\left(\frac{n\pi x}{L} \right) dx,$$

$$B_n = \frac{1}{\sqrt{\lambda_n \frac{c}{\rho}}} \frac{2}{L} \int_0^L v_0(x) \sin\left(\frac{n\pi x}{L} \right) dx, \tag{45}$$

$$\lambda_n = \int_{-\delta}^{\delta} \frac{1}{|\xi|} \left[1 - \cos\left(\frac{n\pi}{L} \xi \right) \right] d\xi,$$

and

$$c = \frac{2E}{\delta^2}$$

5.2 Fixed-Free Boundary Condition

PD EoM, ICs & BCs can be written for fixed-free condition as:

$$\rho\ddot{u}(x,t) = c\int_{-\delta}^{\delta} \frac{u(x+\xi,t)-u(x,t)}{|\xi|} d\xi \quad 0 < x < L \tag{46}$$

$$\text{BCs: } \begin{cases} u(-x,t) = -u(x,t) & 0 \le x \le \delta \\ u(L+x,t) = u(L-x,t) & 0 \le x \le \delta \end{cases} \tag{47a,b}$$

$$\text{ICs: } \begin{cases} u(x,0) = u_0(x) \\ \dot{u}(x,t)\big|_{t=0} = v_0(x) \end{cases} \tag{47a,b}$$

Periodically extending Eq. (47a, b) by imitating Section 4.2 and coupling with (36), one can obtain that

$$a_n = 0 \tag{48a}$$

and

$$s = \frac{2n-1}{2n}\frac{\pi}{L} \tag{48b}$$

Thus, Eq. (36) reduces to

$$u(x,t) = \sum_{n=1}^{\infty}\left[A_n \cos\left(\sqrt{\lambda_n \frac{c}{\rho}}t\right) + B_n \sin\left(\sqrt{\lambda_n \frac{c}{\rho}}t\right)\right]\sin\left(\frac{(2n-1)\pi}{2L}x\right) \tag{49a}$$

and its derivative with respect to t is

$$\dot{u}(x,t) = \sum_{n=1}^{\infty}\sqrt{\lambda_n \frac{c}{\rho}}\left[B_n \cos\left(\sqrt{\lambda_n \frac{c}{\rho}}t\right) - A_n \sin\left(\sqrt{\lambda_n \frac{c}{\rho}}t\right)\right]\sin\left(\frac{(2n-1)\pi}{2L}x\right) \tag{49b}$$

Substituting ICs Eq. (47a, b) into (49a, b) results in

$$u_0(x) = \sum_{n=1}^{\infty} A_n \sin\left(\frac{(2n-1)\pi}{2L}x\right) \tag{50a}$$

and

$$v_0(x) = \sum_{n=1}^{\infty}\sqrt{\lambda_n \frac{c}{\rho}} B_n \sin\left(\frac{(2n-1)\pi}{2L}x\right) \tag{50b}$$

Performing inverse Fourier transform to Eq. (50a,b) determines the coefficients as

$$A_n = \frac{2}{L}\int_0^L u_0(x)\sin\left(\frac{(2n-1)\pi x}{2L}\right)dx \tag{51a}$$

and

$$B_n = \frac{1}{\sqrt{\lambda_n \frac{c}{\rho}}} \frac{2}{L} \int_0^L v_0(x) \sin\left(\frac{(2n-1)\pi x}{2L}\right) dx \tag{51b}$$

Overall, the PD explicit solution for fixed-free problem can be written as:

$$u(x,t) = \sum_{n=1}^{\infty} \left[A_n \cos\left(\sqrt{\lambda_n \frac{c}{\rho}} t\right) + B_n \sin\left(\sqrt{\lambda_n \frac{c}{\rho}} t\right) \right] \sin\left(\frac{(2n-1)\pi}{2L} x\right)$$

with

$$A_n = \frac{2}{L} \int_0^L u_0(x) \sin\left(\frac{(2n-1)\pi x}{2L}\right) dx,$$

$$B_n = \frac{1}{\sqrt{\lambda_n \frac{c}{\rho}}} \frac{2}{L} \int_0^L v_0(x) \sin\left(\frac{(2n-1)\pi x}{2L}\right) dx, \tag{52}$$

$$\lambda_n = \int_{-\delta}^{\delta} \frac{1}{|\xi|} \left[1 - \cos\frac{(2n-1)\pi\xi}{2L} \right] d\xi,$$

and

$$c = \frac{2E}{\delta^2}$$

6. Numerical Results

In this section various numerical cases are presented for both static and dynamic conditions. Different boundary conditions are considered in each case including fixed-fixed boundary condition and fixed-free boundary condition.

6.1. Static Problems

6.1.1 Fixed-Fixed Boundary Condition

In the first case, a bar with a length of L=1m is considered under static conditions. Elastic modulus of the bar is specified as E=200 GPa. The horizon size is chosen as delta=0.01m. The axial loading is applied in the form of f(x)=$1000x(1-x)$.

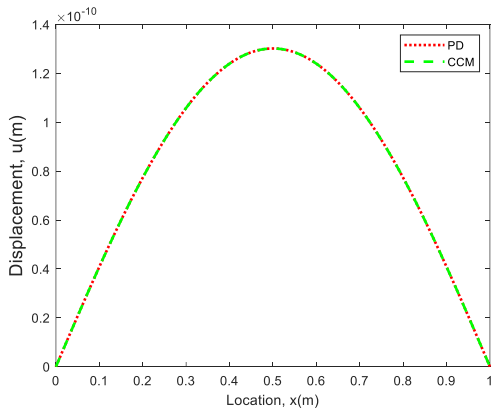

Figure 6. Variation of the axial displacement along the longitudinal bar under fixed-fixed boundary conditions.

The variation of axial displacement along the longitudinal bar from PD is calculated and compared against classical continuum mechanics (CCM) solution. As shown in Fig. 6, a very good agreement is observed between PD and CCM solutions.

6.1.2 Fixed-Free Boundary Conditions

In the second case, the same properties are considered as in the previous case except the boundary condition is chosen as fixed-free boundary condition. The axial displacements obtained from analytical PD solution along the longitudinal bar is compared against CCM solution and a very good match between the two solutions is obtained as shown in Fig. 7.

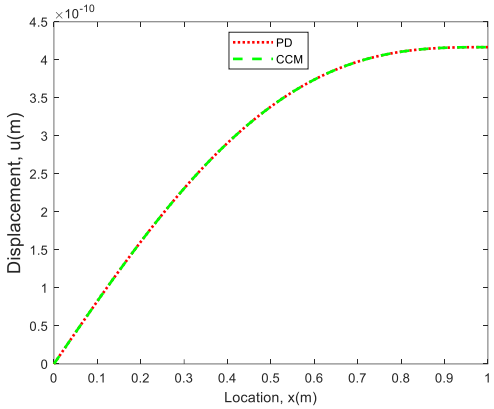

Figure 7. Variation of the axial displacement along the longitudinal bar under fixed-free boundary conditions.

6.2. Dynamic Problems

6.2.1 Fixed-Fixed Boundary Conditions

In this case, a one-dimensional bar with a length of L=1m is utilised. Elastic modulus and density are specified as E=200 GPa and ρ=7850 kg/m^3. The horizon size is chosen as δ=0.01m. Fixed-fixed boundary conditions are considered. Initial conditions are specified as:

ICs: $u_0(x) = 0.01x(x-1)^2$, $v_0(x) = -100x(x-1)^2$

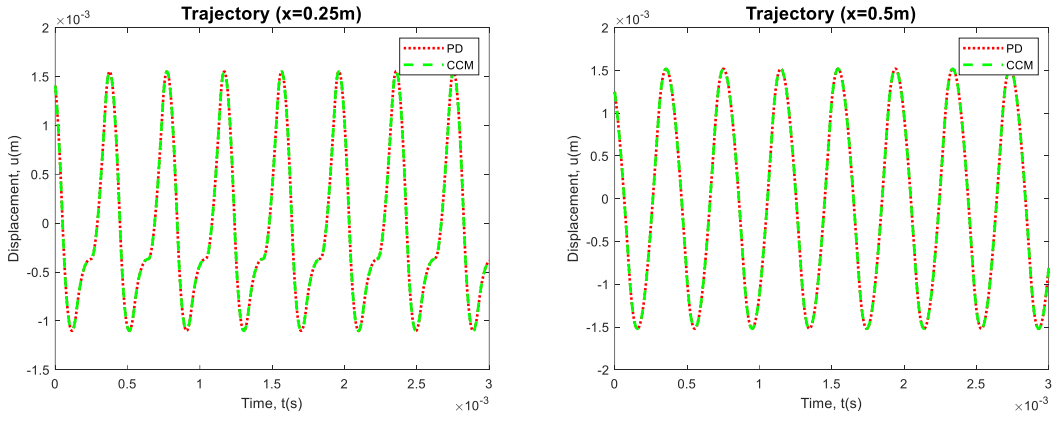

(a) **(b)**

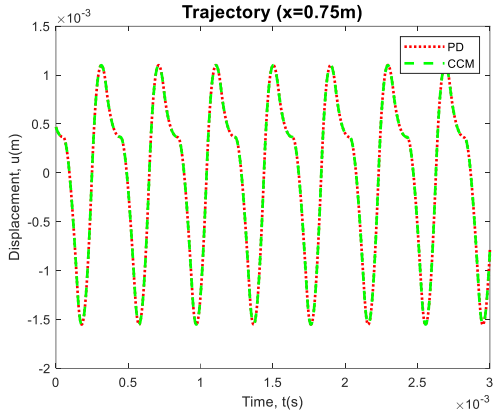

(c)

Figure 8. Variation of the axial displacement with time in the longitudinal bar under fixed-fixed boundary conditions at locations **(a)** x = 0.25 m, **(b)** x = 0.5 m and **(c)** x = 0.75 m.

The variation of axial displacement from analytical PD solution is obtained at three different locations x = 0.25 m, 0.5 m and 0.75 m. As shown in Fig. 8, PD solutions agree very well with CCM results for all three locations.

6.2.2 Fixed-Free Boundary Conditions

In this case, same geometrical and material properties are utilised as in the previous case except boundary conditions are being fixed-free and initial conditions are specified as:

ICs: $u_0(x) = 0.001x$, $v_0(x) = 0$

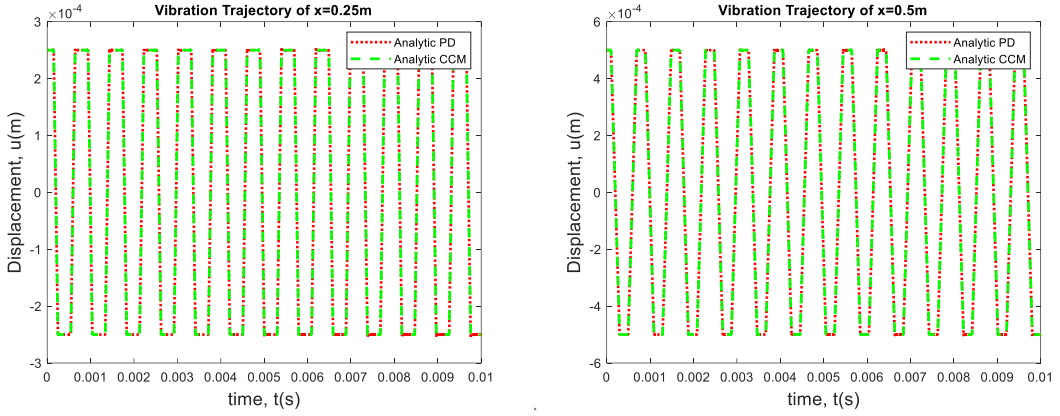

(a) **(b)**

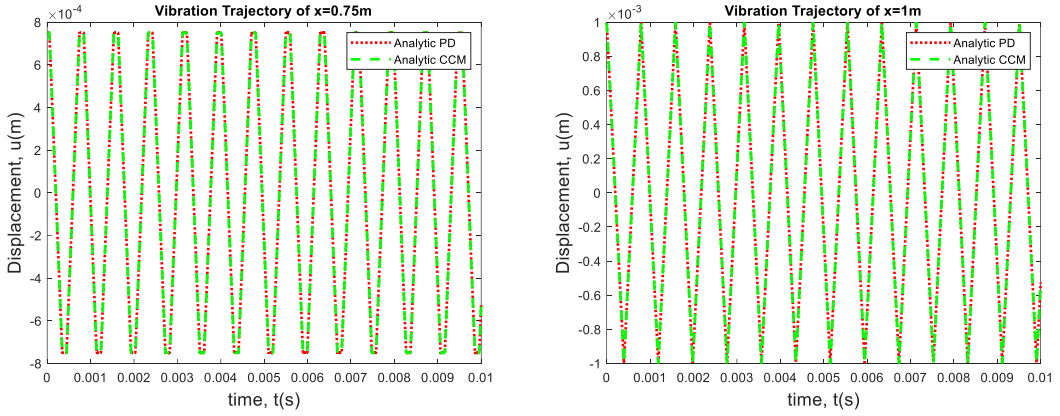

(c) **(d)**

Figure 9. Variation of the axial displacement with time in the longitudinal bar under fixed-free boundary conditions at locations **(a)** x = 0.25 m, **(b)** x = 0.5 m, **(c)** x = 0.75 m and **(d)** x = 1 m.

PD analytical solution for axial displacements at four different locations at x = 0.25 m, 0.5 m, 0.75 m and 1 m are evaluated. By comparing against CCM solutions, it can be concluded that PD solutions match very well with PD solutions as shown in Fig. 9.

6.2.3 Fixed-Free Boundary Conditions

In this case, same geometrical and material properties are utilised as in the previous case except initial conditions are specified as:

ICs:

$u_0(x) = 0.001x^2,\ v_0(x) = 5x^2$

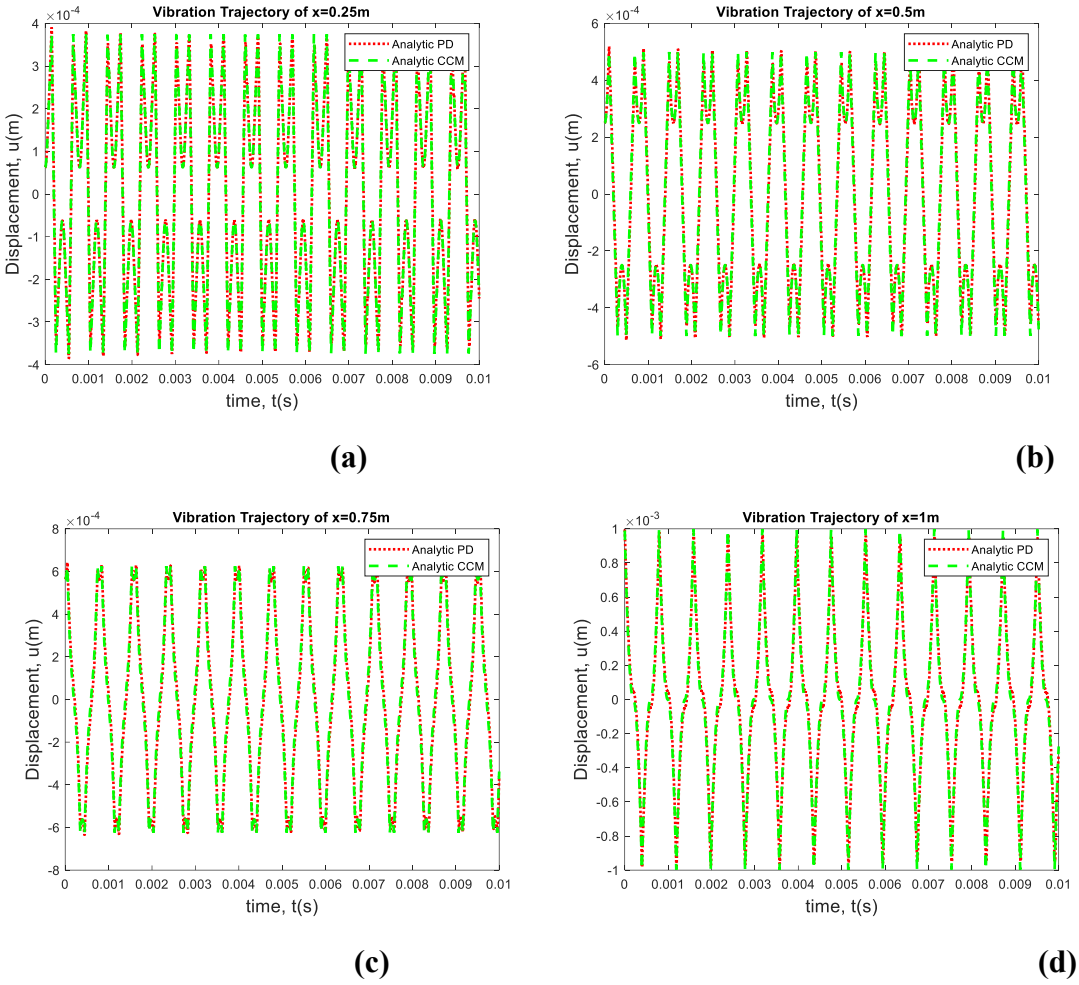

Figure 10. Variation of the axial displacement with time in the longitudinal bar under fixed-free boundary conditions at locations **(a)** x = 0.25 m, **(b)** x = 0.5 m, **(c)** x = 0.75 m and **(d)** x = 1 m.

As demonstrated in Fig. 10, a very good agreement is also observed for this last case between PD and CCM solutions at four different locations x = 0.25 m, 0.5 m, 0.75 m and 1 m.

6.3. Horizon Size Effect

In the third case, the effect of horizon size is investigated by considering a Fixed-Fixed rod with a length of L=1m. Elastic modulus and density are specified as E=200 GPa and ρ=7850 kg/m^3. Different horizon size values are considered as δ=0.005m, 0.05m, 0.07m, 0.1m. The initial conditions are given as:

$$\text{IC: } \begin{cases} u(x,0) = 0.01x^5(x-1)^5 \\ \dot{u}(x,0) = 10x^5(1-x)^5 \end{cases}$$

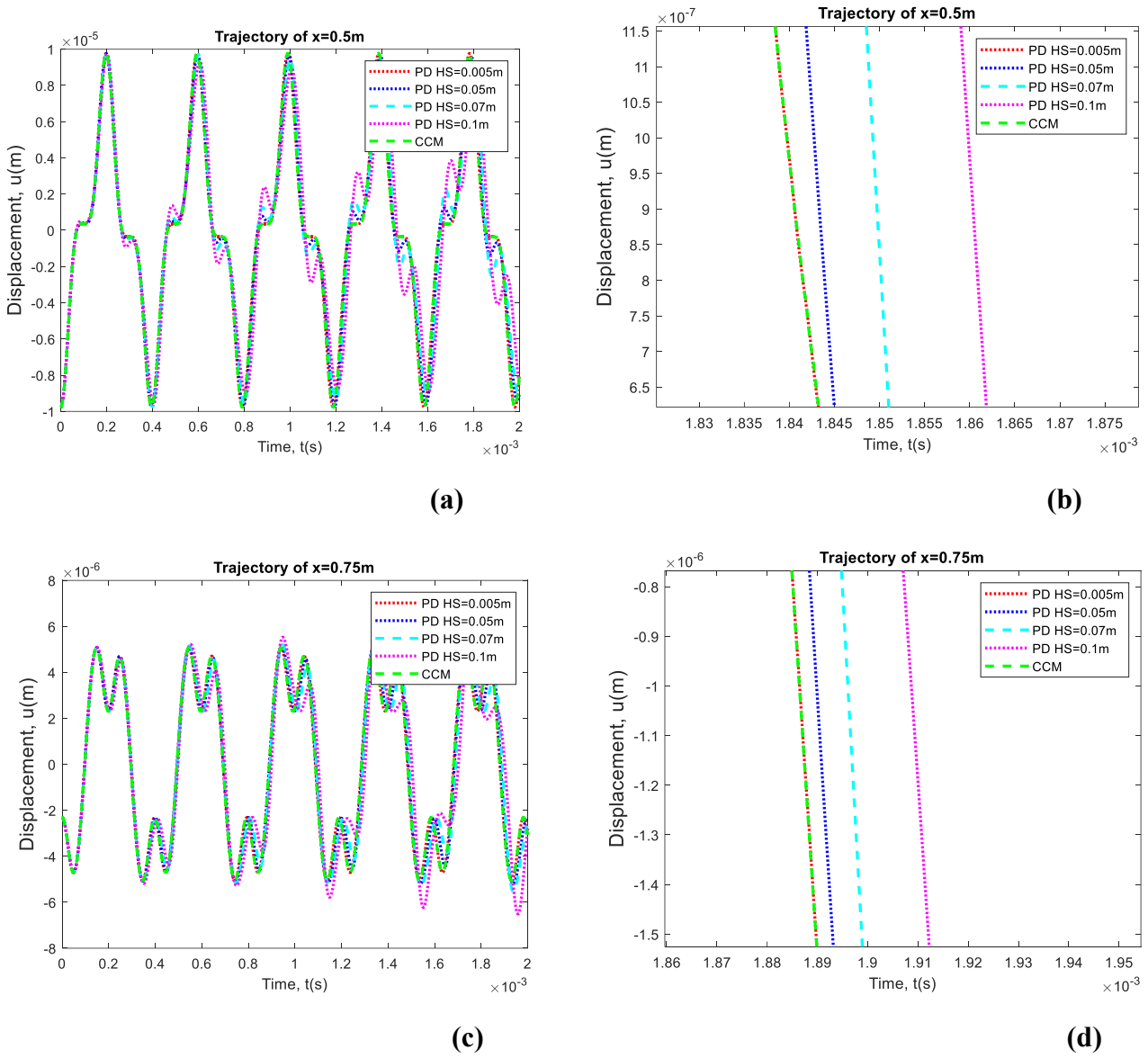

Figure 11. Variation of the axial displacement with time in the longitudinal bar under fixed-fixed boundary conditions at locations **(a)** x = 0.5 m, **(b)** x = 0.5 m (zoomed view), **(c)** x = 0.75 m and **(d)** x = 0.75 m (zoomed view) for different horizon size (HS) values.

Variation of the axial displacement with time in the longitudinal bar at two different locations, x = 0.5 and x = 0.75, are shown in Fig. 11 for different horizon sizes. As can be seen in these figures, as the horizon size is becoming smaller, PD solution is converging to CCM solution which is an expected behaviour.

7. Conclusions

In this study, a new analytical solution methodology is presented by using inverse Fourier Transform for both static and dynamic conditions. Both fixed-fixed and fixed-free boundary conditions are considered. Based on the numerical results generated for both static and dynamic analyses and different boundary and initial conditions, a very good agreement is observed between peridynamic and classical continuum mechanics results. These comparisons verified that the developed new PD analytical model can generate accurate results for different conditions. The current formulation can be extended for the solution of 2-Dimensional peridynamic wave equation.

Data Availability

The datasets generated during and/or analysed during the current study are available from the corresponding author on reasonable request.

References

[1] Silling, S.A., 2000. Reformulation of elasticity theory for discontinuities and long-range forces. *Journal of the Mechanics and Physics of Solids*, *48*(1), pp.175-209.

[2] Madenci, E. and Oterkus, E., 2014. *Peridynamic theory and its applications*. Springer, New York, NY.

[3] Wu, C.T. and Ren, B., 2015. A stabilized non-ordinary state-based peridynamics for the nonlocal ductile material failure analysis in metal machining process. *Computer Methods in Applied Mechanics and Engineering*, *291*, pp.197-215.

[4] Sun, C. and Huang, Z., 2016. Peridynamic simulation to impacting damage in composite laminate. *Composite Structures*, *138*, pp.335-341.

[5] Diyaroglu, C., Oterkus, E., Madenci, E., Rabczuk, T. and Siddiq, A., 2016. Peridynamic modeling of composite laminates under explosive loading. *Composite Structures*, *144*, pp.14-23.

[6] Gerstle, W., Sau, N. and Silling, S., 2007. Peridynamic modeling of concrete structures. *Nuclear engineering and design*, *237*(12-13), pp.1250-1258.

[7] Oterkus, E., Guven, I. and Madenci, E., 2012. Impact damage assessment by using peridynamic theory. *Central European journal of engineering*, *2*(4), pp.523-531.

[8] Cheng, Z., Liu, Y., Zhao, J., Feng, H. and Wu, Y., 2018. Numerical simulation of crack propagation and branching in functionally graded materials using peridynamic modeling. *Engineering Fracture Mechanics*, *191*, pp.13-32.

[9] Ozdemir, M., Kefal, A., Imachi, M., Tanaka, S. and Oterkus, E., 2020. Dynamic fracture analysis of functionally graded materials using ordinary state-based peridynamics. *Composite Structures*, *244*, p.112296.

[10] Silling, S.A., D'Elia, M., Yu, Y., You, H. and Fermen-Coker, M., 2022. Peridynamic Model for Single-Layer Graphene Obtained from Coarse-Grained Bond Forces. *Journal of Peridynamics and Nonlocal Modeling*, pp.1-22.

[11] Liu, X., He, X., Wang, J., Sun, L. and Oterkus, E., 2018. An ordinary state-based peridynamic model for the fracture of zigzag graphene sheets. *Proceedings of the Royal Society A: Mathematical, Physical and Engineering Sciences*, *474*(2217), p.20180019.

[12] Liu, R.W., Xue, Y.Z., Lu, X.K. and Cheng, W.X., 2018. Simulation of ship navigation in ice rubble based on peridynamics. *Ocean Engineering*, *148*, pp.286-298.

[13] Vazic, B., Oterkus, E. and Oterkus, S., 2020. Peridynamic model for a Mindlin plate resting on a Winkler elastic foundation. *Journal of Peridynamics and Nonlocal Modeling*, *2*(3), pp.229-242.

[14] Madenci, E. and Oterkus, S., 2016. Ordinary state-based peridynamics for plastic deformation according to von Mises yield criteria with isotropic hardening. *Journal of the Mechanics and Physics of Solids*, *86*, pp.192-219.

[15] Huang, Y., Oterkus, S., Hou, H., Oterkus, E., Wei, Z. and Zhang, S., 2019. Peridynamic model for visco-hyperelastic material deformation in different strain rates. *Continuum Mechanics and Thermodynamics*, pp.1-35.

[16] Amani, J., Oterkus, E., Areias, P., Zi, G., Nguyen-Thoi, T. and Rabczuk, T., 2016. A non-ordinary state-based peridynamics formulation for thermoplastic fracture. *International Journal of Impact Engineering*, *87*, pp.83-94.

[17] Yang, Z., Oterkus, E. and Oterkus, S., 2021. Peridynamic higher-order beam formulation. *Journal of Peridynamics and Nonlocal Modeling*, *3*(1), pp.67-83.

[18] Dorduncu, M., 2019. Stress analysis of laminated composite beams using refined zigzag theory and peridynamic differential operator. *Composite Structures*, *218*, pp.193-203.

[19] Yang, Z., Vazic, B., Diyaroglu, C., Oterkus, E. and Oterkus, S., 2020. A Kirchhoff plate formulation in a state-based peridynamic framework. *Mathematics and Mechanics of Solids*, *25*(3), pp.727-738.

[20] Naumenko, K. and Eremeyev, V.A., 2022. A non-linear direct peridynamics plate theory. *Composite Structures*, *279*, p.114728.

[21] Dorduncu, M., 2020. Stress analysis of sandwich plates with functionally graded cores using peridynamic differential operator and refined zigzag theory. *Thin-Walled Structures*, *146*, p.106468.

[22] Chowdhury, S.R., Roy, P., Roy, D. and Reddy, J.N., 2016. A peridynamic theory for linear elastic shells. *International Journal of Solids and Structures*, *84*, pp.110-132.

[23] Jung, J. and Seok, J., 2017. Mixed-mode fatigue crack growth analysis using peridynamic approach. *International Journal of Fatigue*, *103*, pp.591-603.

[24] Nguyen, C.T., Oterkus, S. and Oterkus, E., 2021. An energy-based peridynamic model for fatigue cracking. *Engineering Fracture Mechanics*, *241*, p.107373.

[25] Heo, J., Yang, Z., Xia, W., Oterkus, S. and Oterkus, E., 2020. Buckling analysis of cracked plates using peridynamics. *Ocean Engineering*, *214*, p.107817.

[26] Kefal, A., Sohouli, A., Oterkus, E., Yildiz, M. and Suleman, A., 2019. Topology optimization of cracked structures using peridynamics. *Continuum Mechanics and Thermodynamics*, *31*(6), pp.1645-1672.

[27] Imachi, M., Tanaka, S., Ozdemir, M., Bui, T.Q., Oterkus, S. and Oterkus, E., 2020. Dynamic crack arrest analysis by ordinary state-based peridynamics. *International Journal of Fracture*, *221*(2), pp.155-169.

[28] Vazic, B., Wang, H., Diyaroglu, C., Oterkus, S. and Oterkus, E., 2017. Dynamic propagation of a macrocrack interacting with parallel small cracks. *AIMS Materials Science*, *4*(1), pp.118-136.

[29] Diyaroglu, C., Oterkus, S., Oterkus, E., Madenci, E., Han, S. and Hwang, Y., 2017. Peridynamic wetness approach for moisture concentration analysis in electronic packages. *Microelectronics Reliability*, *70*, pp.103-111.

[30] De Meo, D., Russo, L. and Oterkus, E., 2017. Modeling of the onset, propagation, and interaction of multiple cracks generated from corrosion pits by using peridynamics. *Journal of Engineering Materials and Technology*, *139*(4), p.041001.

[31] Shi, C., Gong, Y., Yang, Z.G. and Tong, Q., 2019. Peridynamic investigation of stress corrosion cracking in carbon steel pipes. *Engineering Fracture Mechanics*, *219*, p.106604.

[32] Javili, A., Morasata, R., Oterkus, E. and Oterkus, S., 2019. Peridynamics review. *Mathematics and Mechanics of Solids*, *24*(11), pp.3714-3739.

[33] Mikata, Y., 2012. Analytical solutions of peristatic and peridynamic problems for a 1D infinite rod. *International Journal of Solids and Structures*, *49*(21), pp.2887-2897.

[34] Mikata, Y., 2021. Peridynamics for fluid mechanics and acoustics. *Acta Mechanica*, *232*(8), pp.3011-3032.

[35] Silling, S.A., Zimmermann, M. and Abeyaratne, R., 2003. Deformation of a peridynamic bar. *Journal of Elasticity*, *73*(1), pp.173-190.

[36] Weckner, O. and Abeyaratne, R., 2005. The effect of long-range forces on the dynamics of a bar. *Journal of the Mechanics and Physics of Solids*, *53*(3), pp.705-728.

[37] Weckner, O., Brunk, G., Epton, M.A., Silling, S.A. and Askari, E., 2009. Green's functions in non-local three-dimensional linear elasticity. *Proceedings of the Royal Society A: Mathematical, Physical and Engineering Sciences*, *465*(2111), pp.3463-3487.

[38] Aksoylu, B. and Gazonas, G.A., 2020. On nonlocal problems with inhomogeneous local boundary conditions. *Journal of Peridynamics and Nonlocal Modeling*, *2*(1), pp.1-25.